Synthesis and Analysis of the Density States and Optical Characteristics of $Se_{100-X}Te_X$ Semiconductors

Kassim M. Wadi[1], Maher A. Hasan[2], Shaymaa H. Aneed[3], Mohammad G. Faraj[4] and Kareem A. Jasim[3]

[1]Department of Electrical Engineering Techniques, Al-Ma'amoun University College, Baghdad, F.R. Iraq

[2]Ministry of Education, Tikrit Directorate of Education, Salah Aldin, F.R. Iraq

[3]Department of Physics, College of Education for Pure Sciences ibn Al-Haitham, University of Baghdad, Baghdad, F.R. Iraq

[4]Department of Physics, Faculty of Science and Health, Koya University, Koya KOY45, Kurdistan Region - F.R. Iraq

***Abstract*—The widespread commercial importance of selenium makes it an interesting element. It serves as an effective host matrix for chalcogenide alloys. However, pure selenium has a short lifetime and poor sensitivity. Therefore, specific chemical elements, such as tritium, have been used to overcome this problem. Se-Te alloys are preferred over selenium for their numerous advantages, such as increased electrical sensitivity, thermal stability, and applications in xerography. In this manuscript, the effects of partially substituting tellurium for selenium are studied for amorphous $Se_{100-x}Te_x$ chalcogenide alloys prepared by melt quenching and spraying procedures to produce bulk and thin films, respectively, with varying tellurium concentrations (x = 10, 20, 30, and 40). X-ray diffraction of samples with different concentrations revealed that all samples had an amorphous (glassy) structure. Continuous electrical conductivity is also studied to determine the conduction mechanisms, effective energies, and densities of localized and extended states. The results of electrical conductivity measurements confirm the existence of two conduction modes (extended-state conduction at high temperatures and localized state conduction at intermediate and low temperatures in the tails of the conduction and valence bands). It is also found that the density of states, local and extended state coefficients, and activation energies are significantly affected by the partial substitution of selenium with tellurium. The optical properties of the $Se_{100-x}Te_x$ films are studied using ultraviolet-visible spectroscopy, and it found that the overall absorption increases while the energy gap decreases with increasing tellurium concentration.**

***Index Terms*—Amorphous structure, Chalcogenide, Density of the extended, Electrical measurements, Localized, Optical properties.**

ARO-The Scientific Journal of Koya University
Vol. XIII, No. 1 (2025), Article ID: ARO.11955. 10 pages
DOI: 10.14500/aro.11955
Received: 16 December 2024; Accepted: 20 April 2025
Regular research paper; Published: 05 May 2025
†Corresponding author's e-mail: mohammad.ghaffar@koyauniversity.org

I. Introduction

The development of electronic device technology has required low-cost and competitive materials to support the scientific economy and develop new methods to create a new class of electronic devices made of advanced amorphous materials. Since the production cost of chalcogenide glasses is very low, research has focused on these materials, and a deep understanding of the basic electrical transport properties of materials may provide insight that enhances their merit (Al-Agel, 2011).

Amorphous SeTe semiconductors have gained significant interest due to their high crystallization temperature, high hardness, high photosensitivity, and minimal aging effects compared to pure selenium (Lou, et al., 2012). Doping is one of the most common techniques in amorphous semiconductors, but it is not applicable to pure selenium a-Se due to the Fermi level being fixed by the π states in the band gap (Jouanne, et al., 2004). To modify the optical and electrical properties of a-Se, some additives such as Te, Ge, Bi, Cd, etc. are used, which significantly affect the transport of holes, electrons, or both. In this case, alloying can be considered an effective tool for modifying the electrical transport properties of a-Se films (Chaudhri, Vohra and Chakarvarti, 2008).

Chalcogenide glasses have configurable infrared optical properties and are utilized in numerous modern and logical applications. They are used as gadgets in optical wave gadgets (Tong, 2014; Faraj, 2022), infrared strands (Yang, et al., 2011; Hamad, Faraj and Taha, 2023), sensors (Lucas, et al., 2015, Yang, et al., 2010), optical holes (Elliott, et al., 2010), strong state batteries (Pattanayak, and Asokan, 2005), stage change pens (Elliott, 2015), xerography (Mehta, 2020), and thermoelectrics (Lucas, et al., 2013). Crystalline semiconductor materials are pricey to deliver, and countless scientists resort to concentrating on the properties of materials utilized as alternatives for crystal materials (Borisova, 1981). Such experts have focused

http://dx.doi.org/10.14500/aro.11955

on subtleties and properties of amorphous materials to be used as decisions with a clear plan, and the support for this is the negligible cost from the first viewpoint and then again, the straightforward entry to them. These amorphous semiconductor materials can be consolidated as combinations for their creation and the expansion of specific impurity types to their inefficient electrical conductivity to grow their fields of direction. These different sorts of semiconductors can be utilized in an assortment of semiconductor goods and have various properties. Some are used for standard sign and sun-based cell applications, others in high-recurrence speakers and power applications in brutal conditions, and light-discharging applications. Most applications will utilize various amorphous semiconductor materials, most of which have pitifully fortified layers as the layered units. As in numerous natural analogs, the component of shapeless semiconductors opens the chance of tweaking their electronic properties through neighborhood underlying adjustments. However, the catalysts of these materials are hampered by the structural flexibility of the amorphous lattice, which allows the high formation of favorable coordination defects, called valence and spin (Street and Mott, 1975). Although the effect of the impurities on the electronic properties of amorphous semiconductors is sometimes negative on some properties, it has been proven that alloys containing some chemical elements, such as lead-bismuth and lithium in molten glass, change electrical conductivity (Frumar and Tichý, 1987). This may lead to a reversal of the type of charge carrier, from type p to type n, and maybe vice versa. The n-type conductivity origin in the bismuth-doped chalcogenide glassy has been explained as arising from high bismuth polarization, which partially favors the formation of the ionic bismuth–chalcogen bonds (Elliott and Steel, 1986). In this paper, we will prepare $Se_{100-x}Te_x$ chalcogenide thin film with various tellurium concentrations. Determining the effect of partial replacement elements on structural, electrical, and optical properties is to be studied.

II. Experimental Procedure

Different amounts of ultra-pure selenium and tellurium powder (99.999% from May and Baker LTD Dagenham, England) were mixed according to their molecular weight ratios according to the following equation:

$$(100\text{-}x)\ Se + xTe \rightarrow Se_{100-x}\ Te_x \quad (1)$$

Selenium and tellurium powders of different concentrations (x = 10:20:30:40) were mixed to prepare Se100-xTex alloy samples, and the powder of each sample was placed in quartz glass ampoules. The ampoules were deflated using a vacuum apparatus to 10^{-4} Torr (place the components in a vacuum tube to withstand a temperature of more than 1,200°C so that the elements can react to form alloys without loss or evaporation of the components). The ampoule was sealed tightly and placed in an oven. The oven temperature was raised at a rate of 5°C/min to the melting point. The ampoules were kept in the oven at a high temperature of 600°C for 4 h to melt the components to form the alloy, then heated to 950°C for 12 h to ensure that all the components were melted and to ensure that the samples did not stick to the wall of the ampoules; they were gradually cooled down to 400°C. The ampoules were then removed from the oven to cool; the ampoules were broken, and the alloys were extracted. These alloys were individually ground using a mortar and pestle. The samples were pressed using a hydraulic press under a pressure of seven tons per cm² into discs (2 mm thick and 15 mm in diameter) as shown in Fig. 1.

To conduct electrical tests, the circuits in Fig. 2 were used. The voltage and current data were obtained at different temperatures from room temperature to higher temperatures using a Keithley electrometer. A specially designed holder held the sample between the copper electrodes before applying the two-probe procedure. A copper-constantine thermocouple placed near the sample examined the temperature dependence of the current when a voltage of 9 V was applied. The electrical resistance and electrical conductivity were calculated versus temperature. After that, portions of each sample were taken and ground using an electric grinder for half an hour. After that, the powder of each sample was taken and dissolved in alcohol to prepare

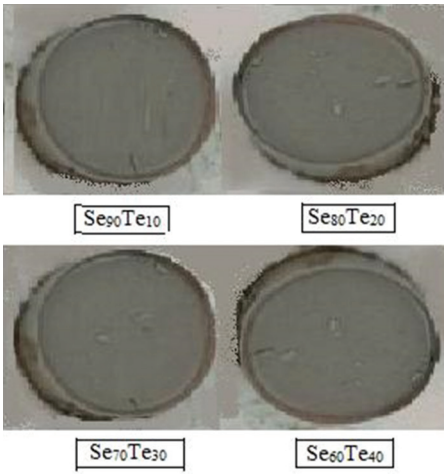

Fig. 1. Images of Se100-xTex chalcogenide samples with different concentrations of tellurium element (x = 10, 20, 30, and 40).

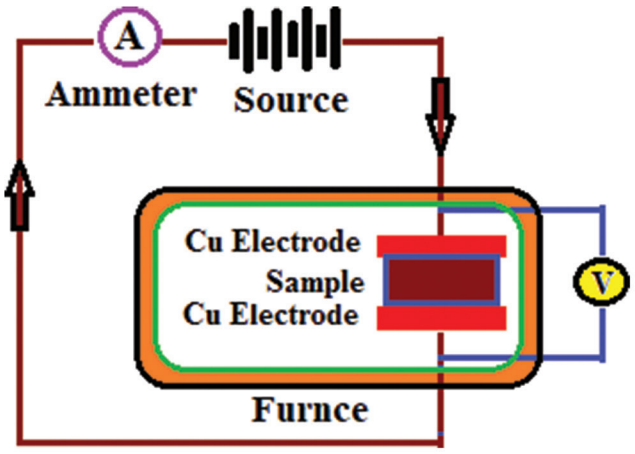

Fig. 2. Schematic diagram of the experimental setup for measuring electrical conductivity.

thin films by spraying them on chalcogenide plates. To prepare the films required in this study, the spraying duration was set to 7 s, after which the spraying was stopped for 2 min, and then the process was repeated since the spraying on the bases could not be continuous. The spray limit is set to 3 min. by using chemical spray pyrolysis, as shown in Fig. 3. The gravimetric method was used to measure the thickness, a technique in which thickness is calculated by measuring the mass, area, and density of the substrate before and after film deposition. The average film thickness (t) is determined using Equation (2).

$$t = 100\frac{W_f}{A_f D_f} \tag{2}$$

Where W_f is the weight difference in micrograms, A_f is the surface area of the substrate having film and D_f is the density of the film. The thicknesses of the samples were of the order of 250 nm.

III. The Theory Parts

Investigating the temperature-dependent electrical conductivity is a well-established technique for investigating how electricity is conducted in random semiconductor materials. According to Davies and Mott, depending on the degree of randomness of the crystal structure, there can be two mechanisms controlling the conduction of electrons and, in some semiconductors with a high randomness structure, up to three mechanisms in other cases (in the Fermi state at low temperatures, at intermediate temperatures (localized states), and at high temperatures (extended states). The general equation below can be used to describe the electrical conductivity of random semiconductors (Mott, Davis, and Street, 1975).

$$\sigma = \sigma_{01} e^{(-\frac{\Delta E_1}{k_B T})} + \sigma_{02} e^{(-\frac{\Delta E_2}{k_B T})} + \sigma_{03} e^{(-\frac{\Delta E_3}{k_B T})} \tag{3}$$

Where ($\sigma_{01,}$ $\sigma_{02,}$ σ_{03}) are represented as pre-exponential factor parameters, (ΔE_1, $\Delta E_{2,}$ ΔE_3) are activation energies for each term, T = the absolute temperature, and k_B = Boltzmann's constant.

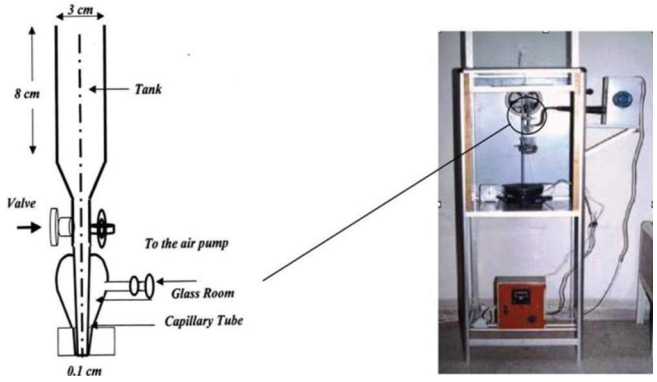

Fig. 3. Experimental set-up of spraying apparatus (right) and layout of enlarged spraying glass nozzle (left).

Some amorphous semiconductors are less random, so they do not have Fermi-level localized states and have two processes (conduction in localized states) at high and intermediate temperatures. In these amorphous materials, the third term in equation 3 is removed, and the equation is given as (Cohen, Fritzsche, and Ovshinsky, 1975).

$$\sigma = \sigma_{01} e^{(-\frac{\Delta E_1}{k_B T})} + \sigma_{02} e^{(-\frac{\Delta E_2}{k_B T})} \tag{4}$$

A. The Electrical Conduction Process throughout Extended States

At high temperatures, continuous electrical conduction through an extended state is the dominant process in the first term of equation 3 (first region). Depending on the activation energy, charge carriers are excited to the denser states in the levels.ΔE_1 where $\Delta E_1 = E_C - E_F$ (or $E_F - E_V$) (Flasck, et al., 1991):

$$\sigma = \sigma_{01} e^{(-\frac{\Delta E_1}{k_B T})} \tag{5}$$

$$\sigma_{01} = \sigma_{0ext} = \left(\frac{1}{6}\right) e^2 a^2 V_e \, N(\text{Eext}) \tag{6}$$

Where e is electron charges, a is atomic distance, and N(Eext) state density at extended state, V_e is the electron frequency and Inter-atomic distance a, therefore the extended state density is:

$$N(E_{ext}) = \left\{ 6m \big/ e^2 \hbar \right\} \sigma_{01} \tag{7}$$

B. The Localized States' Electrical Conduction Processes

This conduction involves the second component of Equation 3, which results in the second conduction mechanism known as in-localized conduction occurring inside the mobility gap. The activation energy in this instance, conduction, results from the transition of charge carriers from the valence band tail states filled with electrons to the levels of the tails of the unoccupied conduction band (Abdulateef, et al., 2020):

$$\sigma = \sigma_{02} e^{(-\frac{\Delta E_2}{k_B T})} \tag{8}$$

$$\sigma_{02} = \left(\frac{1}{6}\right) e^2 V_{ph} R^2 \, N(E_{loc}) \tag{9}$$

Where the phonon frequency (V_{ph} = $10^{13}s^{-1}$), R a hopping distance between localized states (Ahmed, et al., 2022, Chillab, et al., 2021).

$$R = 0.7736 \left\{ \frac{\Delta E \alpha^{-1}}{N(E_{ext})(k_B T)^2} \right\} 25 \tag{10}$$

$$N(E) E_{(LOC)} = \left[\frac{6}{e^2 V_{ph} R^2} \right] \sigma_{02} \tag{11}$$

The energy width tail is $\Delta E = (\Delta E_1 - \Delta E_2)$, and α the absorption coefficient ($\alpha = 10^{-7}$cm) (Ahmed, et al., 2022).

C. Conduction of Electrical Energy (Fermi Level)

The third conduction process, called variable range hopping, or VRH, takes over at lower temperatures by hopping between local states close to the Fermi level (Aqeel, et al., 2020). This kind of tunnel involves the passage of charge carriers via levels that are near the Fermi level. According to the following.

$$\sigma = \sigma_{03} e^{\left(-\frac{\Delta E_3}{k_B T}\right)} \tag{12}$$

$$\sigma_{03} = \left(\frac{1}{6}\right) e^2 V_{ph} R^2 N\left(E_F\right) \tag{13}$$

$$R = \{9/8\left(N\left(E_F\right)\right) B k_B T)\}^{-\frac{1}{4}} \tag{14}$$

Where the localization length of the gap states α^{-1} and N (E_F) is the state density nears the Fermi level (Abdulateef, et al., 2020; Farid, Fadel and Abd El-Wahabb, 2019).

$$N(E_F) = \left[\frac{6}{e^2 Vph\ R^2}\right] \sigma_{03} \tag{15}$$

IV. Results and Discussion

A. Structure Properties

The X-ray diffraction of the studied compositions in powder form is shown in Fig. 4. The obtained patterns indicate that the prepared $Se_{100-x}Te_x$ alloys with various tellurium element concentrations (x = 10, 20, 30 and 40) are in the amorphous state, as no sharp peaks were observed.

B. Electrical Properties

Three processes can lead to electrical conduction in amorphous semiconductors: Charge carrier transitions in the band tails, charge carrier hopping between the Fermi level localized states, and charge carrier transfer between extended states in the conduction and valence bands (Jasim, et al., 2011; Khudhair and Jasim, 2023). In the case of chalcogenide glasses, the electrical conductivity of the charge carriers is either transferred from states near the valence band edge to localized states near the Fermi level or from near the Fermi level to the conduction band.

Fig. 5 shows the DC electrical conductivity variation with temperature of $Se_{100-x}Te_x$ alloys with various element concentrations (x = 10, 20, 30, and 40). It was found that the conductivity increases slowly up to 360 Kelvin and rapidly after 360 Kelvin for all our samples. Charge carriers gain energy when the temperature increases from 300 to 360 Kelvin, where conduction occurs due to the charge carriers jumping in local state bands near the tails of the energy bands. The energy gained for conduction is low due to the decrease in temperature. The same figure shows that the conductivity increases gradually. On the other hand, charge carriers become more mobile, and conduction occurs by the jumping of charge carriers in the conduction band when the temperature increases above 360 Kelvin. As a result, the conductivity increases in the (360–450 Kelvin) temperature range. Therefore, conduction is expected by variable band hopping in the lower temperature range of 300–360 Kelvin, while in the higher temperature range, that is, 360–450 Kelvin, conduction is through a thermally supported process. This Figure clearly shows an increase in continuous electrical conductivity as the temperature rises, indicating that all samples demonstrate semiconductor behavior. In addition, the electrical conductivity increases with increasing tellurium concentration, due to the increase in charge carrier concentrations when tellurium concentrations increase and the decrease in selenium concentration in the prepared samples (Mahdi, et al., 2017).

Fig. 5 demonstrates that the electrical conductivity measurements in all prepared samples have two different states of conductivity: In the extended states, at the

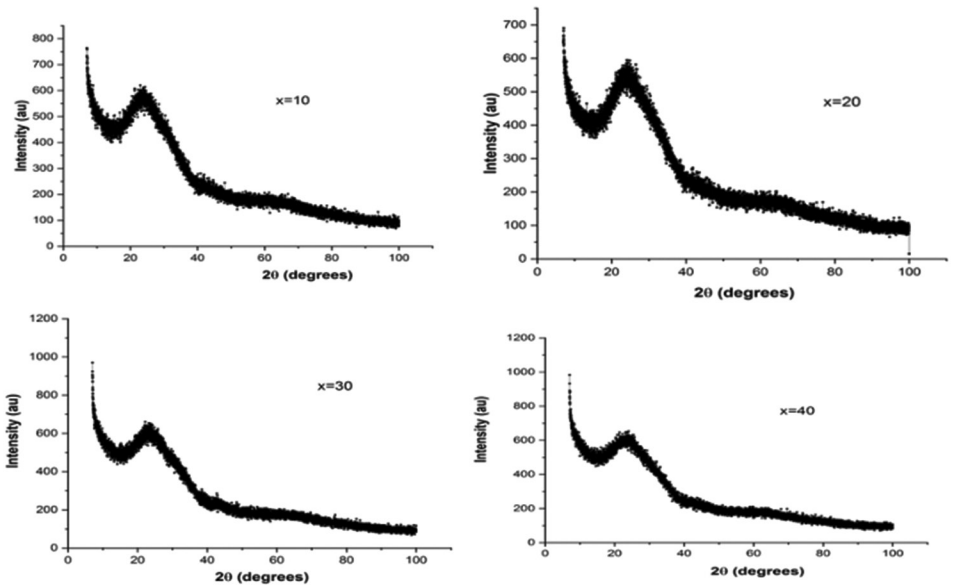

Fig. 4. X-ray diffraction patterns for $Se_{100-x}Te_x$ alloys with various tellurium element concentrations (x = 10, 20, 30, and 40).

temperature, and the average temperature, the conduction was in the local states, and the absence of the local states at the Fermi level. We will be applying equation 4 to carry out the calculations in this instance. As indicated in Table I, the conduction activation (ΔE) and pre-exponential factor (σ_o) of the $Se_{100-x}Te_x$ alloys with different element concentrations (x = 10, 20, 30, and 40) were found using the slope and the intercept plot in the higher temperature range of 348 to 423 Kelvin.

In chalcogenide, the pre-exponential factor (σ_o) provides crucial insights into the coupling mechanism. According to Mott, the pre-exponential factor for coupling in localized states should be two or three orders of magnitude smaller than the coupling factor for extended states (Mohammed and Jasim, 2019). Based on this, we will utilize the equations describing the electrical conductivity in which the conduction mechanisms are limited to the width of the tails and are in the extended condition (Khudhair and Jasim, 2023). To determine both *in situ* and extended state densities, we will apply the equations derived in a theoretical section to data taken from Fig. 5 and recorded in Table I. To calculate densities in the local and extended state, display the tails, and in addition to a part from figuring out the jump distance (R) and the interatomic distance (a). Table I indicates that the prepared alloys do not have energy levels near the Fermi level, indicating that the electrical conductivity of these alloys follows Equation 4. The results of Table I further support this, as they show that the parameters of the exponential factor σ_{01} and σ_{02} preceded the exponent for each sample and have two values. We must use equations 6, 9, and 10 to determine the conduction coefficients necessary to compute the energy state densities for the localized and extended states, respectively.

For all alloys in Table I, the hopping distance R has been computed; the resulting R values are shown in Table II. Fig. 6 shows that the value of hopping distance R typically rises when tellurium concentration rises. However, the increase becomes considerable at x = 40 due to the spacing between the local levels as a result of the partial substitution of selenium by tellurium, which led to a spacing between local energy state levels. This could be explained due to the difference in molecular weight between tellurium and selenium; the molecular weight of tellurium is about 127.6 g/mol, which is larger than the molecular weight of selenium, 78.97 g/mol. This effect will occur when you decrease the ratio of selenium and increase the modifier; the interatomic distance will increase and decrease depending on the modifier ratio. Furthermore, in atomic distance, the increase is due to a change in the sizes of the exchanged atoms (Te =1.36 × 10^{-10} m and Se = 1.16 × 10^{-10} m) as a result of the increase in the concentration of tellurium. This is expected to decrease the density of the local states with the increase of the tellurium concentration (Mohammed, et al., 2023).

The interatomic distance (a) for all alloys and the values are given in Fig. 7 and Table II. From this figure, it can be seen that the interatomic distance value increases in general with increasing concentration of tellurium, but it is clear

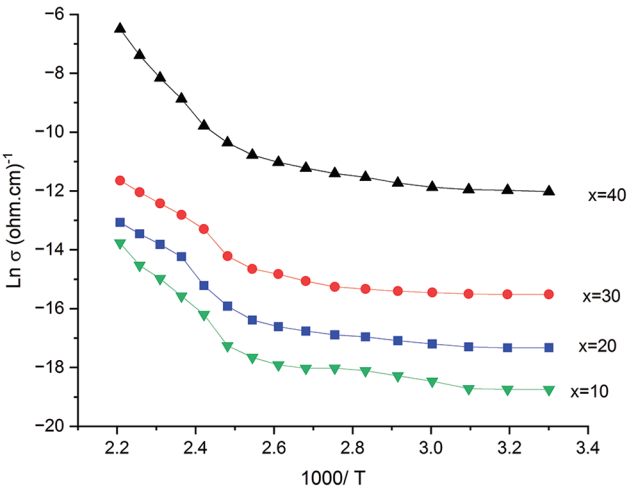

Fig. 5. The change in Ln σ against 1/T for $Se_{100-x}Te_x$ alloys with various Tellurium element concentrations (x = 10, 20, 30 and 40).

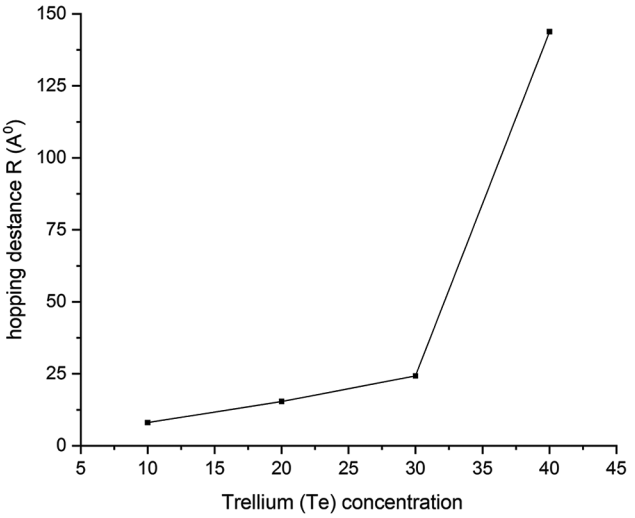

Fig. 6. The value of hopping distance as a function of tellurium (Te) for $Se_{100-x}Te_x$ alloys with various element concentrations (x = 10, 20, 30, and 40).

TABLE I
ELECTRICAL PARAMETERS IN $Se_{100-x}Te_x$ GLASSY SYSTEM AND THE ADDITION OF TELLURIUM AT LOW AND HIGHER TEMPERATURE RANGES

Compositions	ΔE_1	$\sigma_{0ext}(\Omega m)^{-1}$	ΔE_2	$\sigma_{0ext}(\Omega m)^{-1}{}_{\times 10^{-6}}$
$Se_{90}Te_{10}$	0.433	16.3e−2	0.078	0.502
$Se_{80}Te_{20}$	0.380	6.1e−4	0.084	1.16
$Se_{70}Te_{30}$	0.232	3.2e−4	0.094	8.71
$Se_{60}Te_{40}$	0.119	2.9×10^{-5}	0.116	23.7

that this is not the case when x = 40 increases significantly; this is due to the spacing of the atoms becoming too great, which results in a stretched distance between energy levels, which should decrease the density of localized states as the concentration of tellurium increases (Ahmed, et al., 2022).

After calculating interatomic atomic distance (a), tail width (ΔE), and hopping distance (R) from the equations (in the theoretical part, equations 7 and 11), it is easy to

http://dx.doi.org/10.14500/aro.11955

TABLE II
TAIL WIDTH (ΔE), A, R, N (E_{EXT}) AND N (E_{LOC}) AS A FUNCTION OF SE100-XTEX ALLOYS WITH VARIOUS ELEMENT CONCENTRATIONS (X=10, 20, 30, 40)

Compositions	Tail Width (eV)	R (A^0)	a (A^0)	N (E_{ext}) ($ev^{-1}cm^{-3}$)	N (E_{loc})($ev^{-1}cm^{-3}$)	E_g (eV)
$Se_{90}Ge_{10}$	0.355	8.037	6.6	5.73×10^{16}	3.54×10^{8}	2.4
$Se_{80}Ge_{20}$	0.296	15.37	10.29	3.429×10^{15}	5.78×10^{8}	1.8
$Se_{70}Ge_{30}$	0.138	24.25	14.73	4.723×10^{15}	2.68×10^{9}	2
$Se_{60}Ge_{40}$	0.083	143.8	17.68	9.38×10^{12}	1.485×10^{10}	1.7

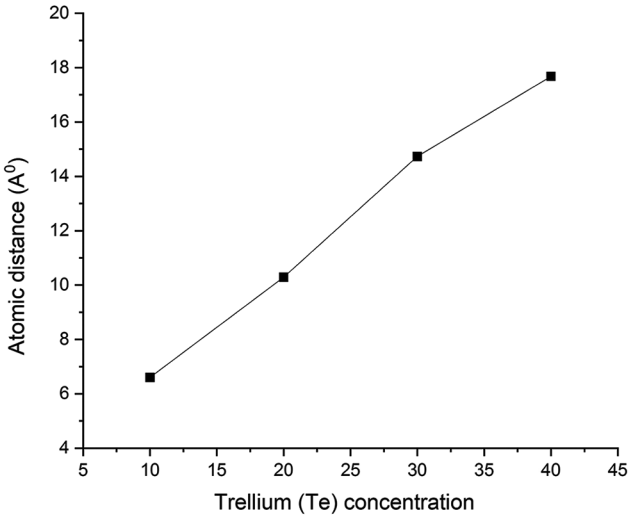

Fig. 7. The value of interatomic distance as a function of tellurium (Te) for $Se_{100-x}Te_x$ alloys with various element concentrations (x = 10, 20, 30, and 40).

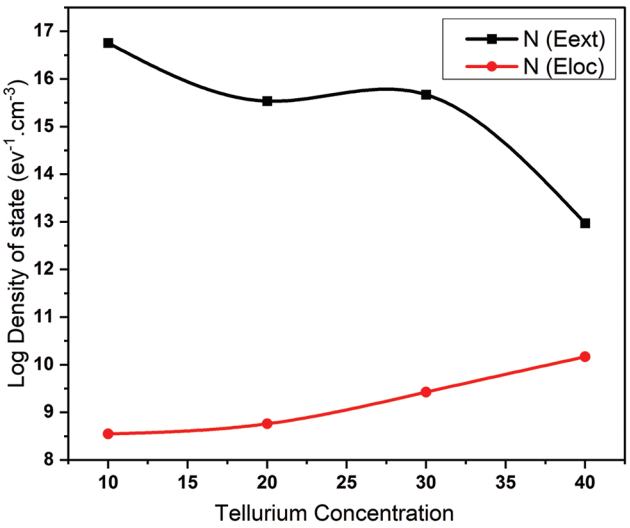

Fig. 8. The tellurium concentration-dependent value of the energy density of extended and localized states for $Se_{100-x}Te_x$ alloys with various element concentrations (x = 10, 20, 30, and 40).

calculate the localized and extended states density for energy. Calculating densities of localized N (E_{loc}) and extended N (E_{ext}) states requires knowledge of the pre-exponential factor parameters σ_{0loc} and σ_{0ext} in the region of these states, whose values for each alloy are listed in Table I. The extended state density is calculated using equation 5, while the local density of states N (E_{loc}) at the tails of the bands inside the mobility energy gap is calculated using equations 6, respectively, after substitution for σ_{0ext}, σ_{0ext}, Tail Width ΔE, R and inter-atomic distance (a). Table II displays the tabulated results, which are scheduled.

Fig. 8 demonstrates the relation between the energy localized density N (E_{loc}) and extended N (E_{ext}) states as a function of tellurium concentration (Te), where it was observed based on this form that the extended density state decreased from 5.73×10^{16} to 9.38×10^{12} ($ev^{-1}cm^{-3}$), with the increasing tellurium concentration from 10 to 40. The density of the localized state increases from 3.54×10^{8} until it reaches a large value (1.485×10^{10} $ev^{-1}cm^{-3}$). This change is due to the energetic activation, as shown in Fig. 8 and Tables I and II. The increase in the density of the local states at the tails of the bundles inside the kinetic energy gap and the decrease in the density of the stretched states indicate that some energy levels in the conduction and valence bands slipped, forming tails inside the energy gap, and in this case, it caused an increase in the randomness of crystal structure samples with the increase in concentration of tellurium (Aqeel, et al., 2020).

C. Optical Proprieties

The study of optical properties has provided important information about semiconductor materials and their potential. They are used in various practical applications, and the optical behavior of semiconductor materials is related to their shape. It is closely related to the structure of energy levels, which is associated with matter's crystalline structure.

Absorptance (A)

The absorption coefficient, which is symbolized by the symbol (α), is defined as the percentage decrease in the flux of radiation energy per unit distance in the direction of the wave propagation within the medium (Patil, et al., 2004). It depends on the energy of the photons and their wavelength, as well as the nature of the surface of the thin film and the energy gap of the semiconductor, as well as the type of electronic transfers that occur. Between energy beams, the absorption coefficient was calculated from the relationship (Jacques, 1975).

$$\alpha = (2.303\ A)/t \quad (16)$$

Where α: absorption coefficient, t: membrane thickness, A: Absorption.

Fig. 9 shows the change in absorbance (A) as a function of the incident photon energy for the $Se_{100-x}Te_x$ with x = 10, 20, 30, and 40. It is noted that the absorbance values are very low for the $Se_{90}Te_{10}$ sample membrane because the incident photons It was not able to excite the electrons and

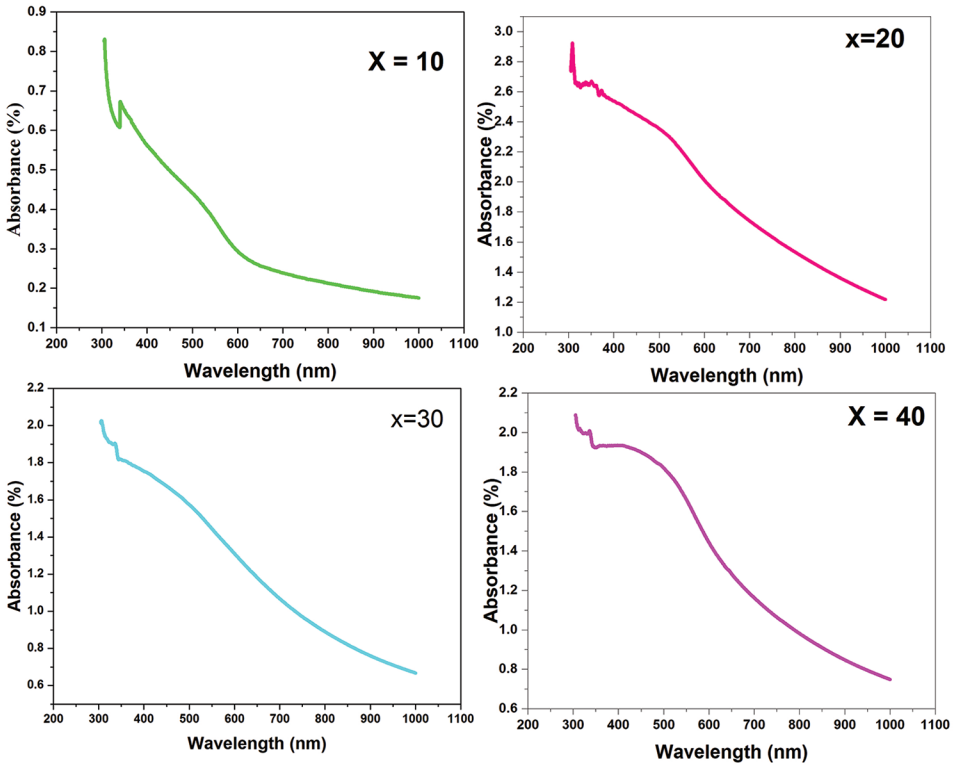

Fig. 9. Absorbance as a function of the wavelength of the $Se_{100-x}Te_x$ thin films with various element concentrations (x = 10, 20, 30, and 40).

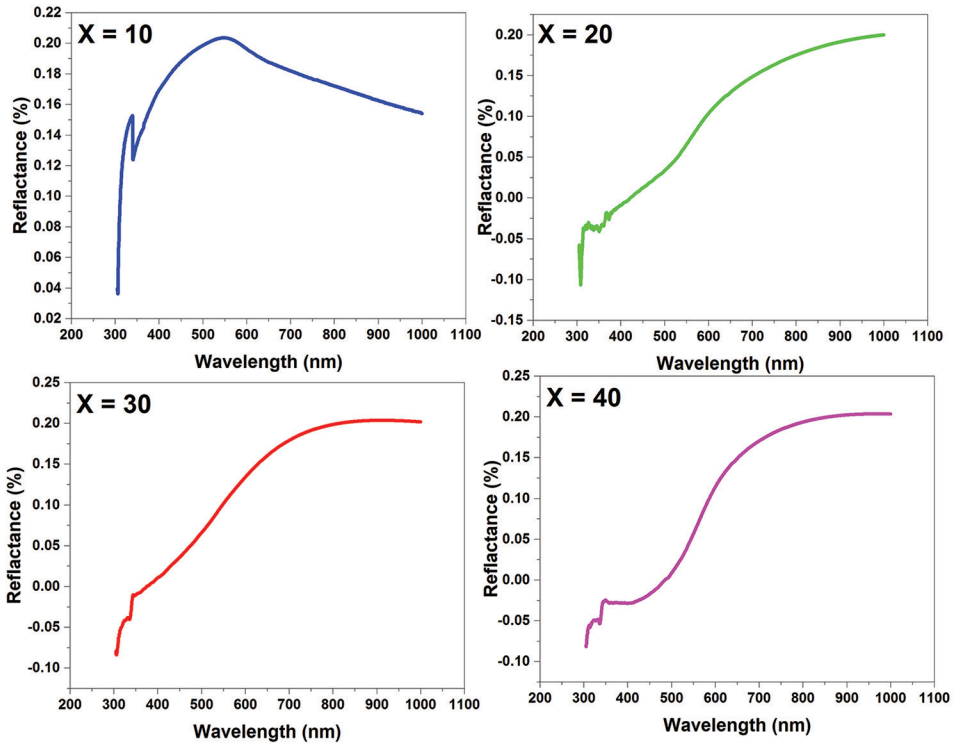

Fig. 10. Reflectance (R) is a function of the wavelength of the $Se_{100-x}Te_x$ thin films with various element concentrations (x = 10, 20, 30, and 40).

move them from the valence band to the conduction band because the photon energy is less than the value of the optical energy gap of the semiconductor and continues to decrease with the increase in the energy of the incident light photons until it reaches its peak and becomes almost constant, when the energy of the incident photons becomes equal to or greater than the energy gap (Lanyon, 1964). After that, we also notice from the figure that the absorbance of the samples in which the tellurium element concentrations increase behaves in the same way as the energy of the incident photon increases, except

http://dx.doi.org/10.14500/aro.11955

that the absorbance spectrum of the membranes increases with the increase in the concentration of Te, due to the occurrence of absorption processes mediated by levels. The resulting inoculation of tellurium increases absorbency, accompanied by sharp edges (absorption edge) displacement toward lower energies with increasing concentration. It is also noted from the figure that the basic absorption edge (the border between the high light absorption region and the transparent region) for all samples ranges between 300 and 1000 nm. We also note that the absorption coefficient for all cases has values $>10^4$ in the high energy range, and this agrees with the references (Abd-Elrahman, et al., 2013; Al-Agel, 2013).

Reflectance

Reflectivity (R) can be defined as the ratio of the amount of energy that is reflected during the beam's incident on the surface of the thin film to the amount of power of the incident beam (Yang, et al., 2010). The reflectivity was calculated from the absorbance and transmittance spectra according to the law of conservation of energy according to the relationship:

$$A + T + R = 1 \quad (17)$$

$$R = 1 - A - T \quad (18)$$

Fig. 10 shows the reflectivity as a function of wavelength for membrane $Se_{100-x}Te_x$ alloys with various element concentrations (x = 10, 20, 30, and 40), and we notice from the figure that the reflectivity generally increases with increasing wavelength for short wavelengths. The reflectance is high in near-infrared and near visible regions. According to these results, the films are suitable for solar control coatings.

The following relationships can be used to calculate optical constants, including the extinction coefficient e_υ, the refractive index n:

$$e_\upsilon = \frac{\alpha\lambda}{4\pi} \quad (19)$$

$$n = \left[\frac{4R}{(1-R)^2} - e_\upsilon^{,2}\right]^{1/2} - \frac{(1+R)}{(1-R)} \quad (20)$$

Fig. 11 represents the relationship between the refractive index and the change in wavelength of the $Se_{100-x}Te_x$ thin films with various element concentrations (when x = 10, 20, 30, and 40). It is noted that the refractive index values of all the prepared films are high at short wavelengths, between 300 and 450 nm. However, when we reach approximately the wavelength (λ = 500 to 550 nm), we observe a significant decrease in the refractive index due to reaching the absorption edge, reaching its lowest value at energy values corresponding to the optical energy gap for all the films under investigation. This behavior is attributed to the increased number of direct electronic transitions at these energies (Reddy and Bhatnagar, 1992; Abd-Elrahman, et al., 2013; Al-Agel, 2013).

Energy gap

Relationship (21) was used to calculate the energy gap.

$$\alpha h\upsilon = A\,(h\upsilon - Eg)^{1/2} \quad (21)$$

Where: α- absorption coefficient: hυ - photon energy: A- constant, and E_g = energy gap:

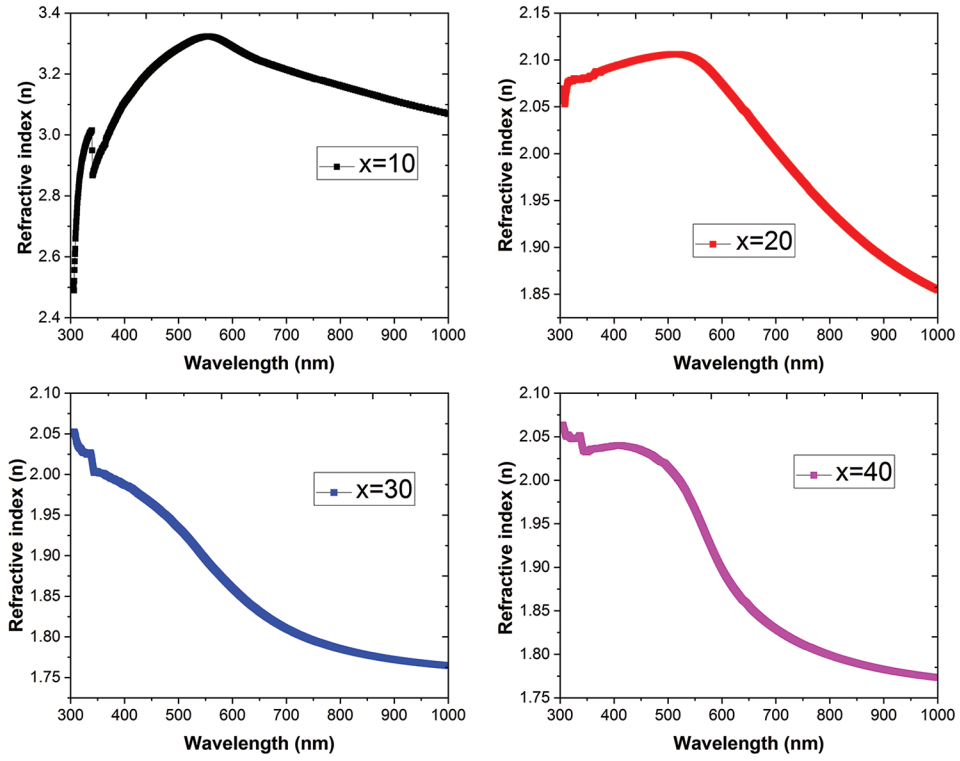

Fig. 11. Refractive Index is a function of the wavelength of the $Se_{100-x}Te_x$ thin films with various element concentrations x = 10, 20, 30, and 40.

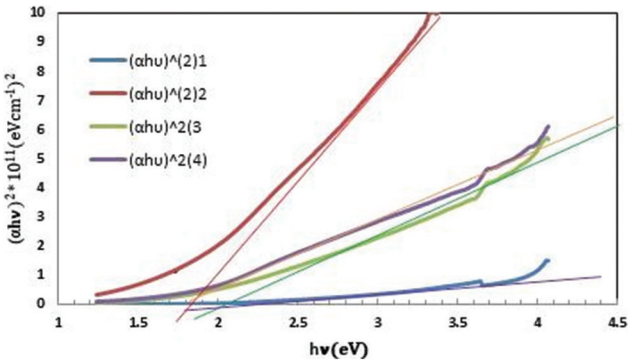

Fig. 12. (a hν)² a function of the photon energy of the $Se_{100-x}Te_x$ thin films with various element concentrations (x = 10, 20, 30, and 40).

The graphic relationship was drawn between (α hυ)² and the photon energy (hυ) to determine the energy gap. It is clear from Fig. 12 that the value of F The energy value ranged from 1.7 to 2.4 eV. As shown in Table II, it becomes clear to us that the partial replacement of selenium with tellurium led to a change in the value of the energy gap, and the explanation for this decrease is that increasing the concentration of tellurium led to the generation of additional energy levels within the prohibited gap (Street and Mott, 1975). Proximity to the conduction beam leads to a reduction in photon energy required for direct electron transfers, which makes the transfer of electrons from the valence band to the conduction band easier.

V. Conclusion

In the above sections, we analyzed the electrical conductivity in Se100-xTex amorphous chalcogenide films with different concentrations. The I-V characteristics of the amorphous thin films prepared by the melting point method were obtained in the temperature range (300–423 K). The characteristics showed a transition from an ohmic region at a low applied voltage to a non-linear region at a higher voltage. There are two specific regions of conduction in the extended state at high temperatures and conduction in the localized state at medium and low temperatures in the tails of the conduction and valence bands. The behavior of the non-ohmic region of the electrical resistivity characteristics can be understood in terms of the temperature dependence of the ohmic current with a thermal activation process with a single activation energy for each sample. The density of the localized and extended states was calculated, and it was found that there was a clear change with increasing selenium concentration. The activation energy and absorbance values were studied for each of the $Se_{100-x}Te_x$ amorphous films.

References

Abd-Elrahman, M.I., Khafagy, Rasha M., Zaki, S.A., and Hafiz, M.M., 2013. Effect of composition on the optical constants of $Se_{100-x}Te_x$ thin films. *Journal of Alloys and Compounds*, 571, pp.118-122.

Abdulateef, A.N., Alsudani, A., Chillab, R.K., Jasim, K.A., and Shaban, A.H., 2020. Calculating the mechanisms of electrical conductivity and energy density of states for $Se_{85}Te_{10}Sn_{5-x}In_x$ glasses materials. *Journal of Green Engineering*, 10, pp.5487-5503.

Ahmed, B.A., Mohammed, J.S., Fadhil, R.N., Jasim, K.A., Shaban, A.H., and Al Dulaimi, A.H., 2022. The dependence of the energy density states on the substitution of chemical elements in the $Se_6Te_{4-x}Sb_x$ thin film. *Chalcogenide Letters*, 19, pp.301-308.

Al-Agel, F.A., 2011. Influence of composition on electrical and optical properties of new chalcogenide thin films from Ge-Se-Tl system. *Optics and Laser Technology*, 43, pp.781-786.

Al-Agel, F.A., 2013. Optical and structural properties of amorphous Se_xTe_{100-x} aligned nanorods. *Nanoscale Research Letters*, 9, pp.520.

Borisova, Z.U.U., 1981. In: Adashko, J.G., Ed. *Glassy Semiconductors*. Springer Science and Business Media, LLC.

Chaudhri, M., Vohra, A., and Chakarvarti, S.K., 2008. Fabrication of Zn/Cd-Se micro heterostructures by electrochemical deposition in the pores of polycarbonate track-etch membranes and their characterization. *Physica E: Low-Dimensional Systems and Nanostructures*, 40, pp.849-851.

Chillab, R.K., Jahil, S.S., Wadi, K.M., Jasim, K.A., and Shaban, A.H., 2021. Fabrication of $Ge_{30}Te_{70-x}Sb_x$ glasses alloys and studying the effect of partial substitution on d.C electrical energy parameters. *Key Engineering Materials*, 900, pp.163-171.

Cohen, M.H., Fritzsche, H., and Ovshinsky, S.R., 1969. Simple band model for amorphous semiconducting alloys. *Physical Review Letters*, 22(20), pp.1065-1068.

Elliott, G.R., Murugan, G.S., Wilkinson, J.S., Zervas, M.N., and Hewak, D.W., 2010. Chalcogenide glass microsphere laser. *Optics Express*, 18, pp.26720-26727.

Elliott, S.R., 2015. Chalcogenide phase-change materials: Past and future. *International Journal of Applied Glass Science*, 6, pp.15-18.

Elliott, S.R., and Steel, A.T., 1986. Mechanism for doping in Bi chalcogenide glasses. *Physical Review Letters*, 57, pp.1316-1319.

Faraj, M.G., 2022. Effect of substrate temperature on the electrical properties of al-doped zinc oxide films deposited on polyethylene terephthalate. *Aro-The Scientific Journal of Koya University*, 10, pp.131-133.

Farid, A.S., Fadel, M., and Abd El-Wahabb, E., 2019. AC electrical conductivity and dielectric relaxation behavior of amorphous Se36In31Cu33 thin films. *Phase Transitions*, 92, pp.1031-1042.

Flasck, R., Izu, M., Sapru, K., Anderson, T., Ovshinsky, S.R., and Fritzsche, H., 1991. Optical and electronic properties of modified amorphous materials. *Disordered Materials*, pp.51-53.

Frumar, M., and Tichý, L., 1987. N-type conductivity in chalcogenide glasses and layers. *Journal of Non-Crystalline Solids*, 97-98, pp.1139-1146.

Hamad, N.H., Faraj, M.G., and Taha, A.H., 2023. Structural and optical properties of cadmium sulfide-doped silver deposited on glass and polymer substrates by chemical spray pyrolysis. *Aro-The Scientific Journal of Koya University*, 11, pp.32-37.

Jacques, I.P., 1975. *Optical Processes in Semiconductors*. Dove Publications lnc., New York.

Jasim, K.A., Alwan, T.J., Al-Lamy, H.K., and Mansour, H.L, 2011. Improvements of superconducting properties of hg0.6pb0.25sb0.15ba2ca2cu3o8+δ ceramic by controlling the sintering time. *Journal of Superconductivity and Novel Magnetism*, 24, pp.1963-1966.

Jouanne, M., Morhange, J.F., Dynowska, E., Łusakowska, E., Szuszkiewicz, W., Molenkamp, L.W., and Karczewski, G., 2004. Structure characterization of MBE-grown (Zn, Cr) Se layers. *Journal of Alloys and Compounds*, 32, pp.92-99.

Khudhair, N.H., and Jasim, K.A., 2023. Study the effect of tin on the energy density of states Se60Te40-xSnx chalcogenide glass. *AIP Conference Proceedings*, 2769, p.020062.

Khudhair, N.H., and Jasim, K.A.A., 2023. Study of the effectiveness of tin on the thermal conductivity coefficient and electrical resistance of Se60Te40-xSnx chalcogenide glass. *Ibn AL-Haitham Journal for Pure and Applied Sciences*, 36, pp.149-157.

Lanyon, H.P.D., 1964. Optical and electrical properties of selenium-tellurium alloys. *Journal of Applied Physics*. 35, pp.1516-1523.

Lou, S., Zhou, C., Xu, W., Wang, H., Zhou, S., Shen, H., and Li, L.S., 2012. Facile synthesis of water-soluble $Zn_xCd_{1-x}Se$ nanocrystals via a two-phase cation exchange method. *Chemical Engineering Journal*, 211-212, pp.104-111.

Lucas, P., Coleman, G.J., Jiang, S., Luo, T., and Yang, Z., 2015. Chalcogenide glass fibers: Optical window tailoring and suitability for bio-chemical sensing. *Optical Materals*, 47, pp.530-536.

Lucas, P., Conseil, C., Yang, Z., Hao, Q., Cui, S., Boussard-Pledel, C., Bureau, B.,Gascoin, F.,Caillaud, C., Gulbiten, O., Baruah, P., Guizouarn, T., Li, Q., and Lucas, J., 2013. Thermoelectric bulk glasses based on the Cu-As-Te-Se system. *Journal of Materials Chemsitry A*, 1, p.31.

Mahdi, S.H., Jassim, W.H., Hamad, I.A., and Jasima, K.A., 2017. Epoxy/silicone rubber blends for voltage insulators and capacitors applications. *Energy Procedia*, 119, pp.501-506.

Mehta, N., 2020. Recent applications of chalcogenide glasses (ChGs) based sensors. In: *Advances in Modern Sensors*. IOP Science, United Kingdom.

Mohammed, J.S., Nsaif, F.K., Jawad, Y.M., Jasim, K.A., and Al Dulaimi, A.H., 2023. Investigating the optical and electrical characteristics of As60Cu40-xSex thin films prepared using pulsed laser deposition method. *Chalcogenide Letters*, 20, pp.449-458.

Mohammed, L.A., and Jasim, K.A., 2019. Improvement the superconducting properties of $TlBa_2$ Ca_2 Cu_{3x} Ni_x $O_{9-\delta}$ superconducting compound by partial substitution of copper with nickel oxide on the. *Energy Procedia*, 157, pp.135–142.

Mott, N.F., Davis, E.A., and Street, R.A., 1975. States in the gap and recombination in amorphous semiconductors. *Philosophical Magazine*, 32, pp.961-996.

Patil, V., Shahane, G., Sutrave, D., Raut, B., and Deshmukh, L., 2004. Photovoltaic properties of N-CdS1-xTex thin film/oxysulphide photoelectrochemical solar cells prepared by chemical bath deposition. *Thin Solid Films*, 446, pp.1-5.

Pattanayak, P., and Asokan, S., 2005. Signature of a silver phase percolation threshold in microscopically phase separated ternary Ge0.15Se0.85-XAgx ($0 \geq x \geq 0.20$) glasses. *Journal of Applied Physics*, 97, pp.13-16.

Reddy, K.V., and Bhatnagar, A.K., 1992. Electrical and optical studies on amorphous Se-Te alloys. *Journal of Physics D: Applied Physics*, 25, pp.1810.

Street, R.A., and Mott, N.F., 1975. States in the gap in glassy semiconductors. *Physical Review Letters*, 35, pp.1293-1296.

Tong, X.C., 2014. *Advanced Materials for Integrated Optical Waveguides*. Springer Science and Business Media, Germany.

Yang, Z., Fah, M.K., Reynolds, K.A., Sexton, J.D., Riley, M.R., Anne, M.L., Bureau, B., and Lucas, P., 2010. Electrophoretic detection of bio-molecules using conducting chalcogenide glass sensors. *Optics Express*, 18, pp.26754-26759.

Yang, Z., Gulbiten, O., Lucas, P., Luo, T., and Jiang, S., 2011. Long-wave infrared-transmitting optical fibers. *Journal American Ceramic Society*, 94, pp.1761-1765.